




Article

Pure and Fe-Doped Mesoporous Titania Catalyse the Oxidation of Acid Orange 7 by H₂O₂ under Different Illumination Conditions: Fe Doping Improves Photocatalytic Activity under Simulated Solar Light

Francesca S. Freyria^{1,2}, Matteo Compagnoni³, Nicoletta Ditaranto⁴ , Ilenia Rossetti³ , Marco Piumetti¹, Gianguido Ramis⁵ and Barbara Bonelli^{1,2,*} 

¹ Department of Applied Science and Technology Politecnico di Torino, Corso Duca degli Abruzzi, 24, 10129 Torino, Italy; francesca.freyria@polito.it (F.S.F.); marco.piumetti@polito.it (M.P.)

² INSTM Unit of Torino-Politecnico, Corso Duca degli Abruzzi, 24, 10129 Torino, Italy

³ Dipartimento di Chimica, Università degli Studi di Milano, CNR-ISTM and INSTM Unit Milano-Università, via C. Golgi 19, 20133 Milano, Italy; matteo.compagnoni@unimi.it (M.C.); ilenia.rossetti@unimi.it (I.R.)

⁴ Dipartimento di Chimica, Università degli Studi di Bari “Aldo Moro”, via Orabona 4, 70125 Bari, Italy; nicoletta.ditaranto@uniba.it

⁵ Dipartimento di Ingegneria Chimica, Civile ed Ambientale, Università degli Studi di Genova and INSTM Unit Genova, P.le Kennedy 1, 16129 Genova, Italy; gianguidoramis@unige.it

* Correspondence: barbara.bonelli@polito.it; Tel.: +39-011-090-4719

Academic Editor: Adam F. Lee

Received: 5 May 2017; Accepted: 11 July 2017; Published: 18 July 2017

Abstract: A sample of mesoporous TiO₂ (MT, specific surface area = 150 m²·g⁻¹) and two samples of MT containing 2.5 wt.% Fe were prepared by either direct synthesis doping (Fe2.5-MTd) or impregnation (Fe2.5-MTi). Commercial TiO₂ (Degussa P25, specific surface area = 56 m²·g⁻¹) was used both as a benchmark and as a support for impregnation with either 0.8 or 2.5 wt.% Fe (Fe0.80-IT and Fe2.5-IT). The powders were characterized by X-ray diffraction, N₂ isotherms at −196 °C, Energy Dispersive X-ray (EDX) Spectroscopy, X-ray Photoelectron Spectroscopy (XPS), Diffuse Reflectance (DR) ultra-violet (UV)-Vis and Mössbauer spectroscopies. Degradation of Acid Orange 7 (AO7) by H₂O₂ was the test reaction: effects of dark-conditions versus both UV and simulated solar light irradiation were considered. In dark conditions, AO7 conversion was higher with MT than with Degussa P25, whereas Fe-containing samples were active in a (slow) Fenton-like reaction. Under UV light, MT was as active as Degussa P25, and Fe doping enhanced the photocatalytic activity of Fe2.5-MTd; Fe-impregnated samples were also active, likely due to the occurrence of a photo-Fenton process. Interestingly, the Fe2.5-MTd sample showed the best performance under solar light, confirming the positive effect of Fe doping by direct synthesis with respect to impregnation.

Keywords: mesoporous titania; soft-template synthesis; azo dyes; iron doping; Fenton reaction; photo-Fenton reaction; photocatalysis; solar light

1. Introduction

TiO₂ is a widely used semiconductor due to its band gap (3.2–3.0 eV), low toxicity, availability of different polymorphs and the possibility to obtain TiO₂ nanoparticles (NPs) with different morphologies and shapes [1–3]. Such physico-chemical properties promote the use of TiO₂ mostly as photocatalyst and/or a catalytic support [3–7], although it is also used in dye sensitized solar cells [8–11] and, recently, in biomedical applications [12,13]. Moreover, the possibility of obtaining ordered porous structures with remarkable specific surface area (SSA) enhances the use of TiO₂ in

(photo)catalysis as the presence of ordered mesoporous channels promotes the diffusion of both reactants and products by facilitating access to surface reactive sites [4,14].

Concerning photocatalytic processes, one of the polymorphs of TiO_2 , i.e., anatase, is along with BiVO_4 and WO_3 [15] one of the most studied semi-conductors in the search for the artificial leaf, i.e., a system able to “mimic” the behavior of plants, with the final aim of producing H_2 , a clean energy vector, or of reducing CO_2 to fuels [16–18].

TiO_2 is currently applied for the degradation of persistent organic pollutants [5,6,19–22], including azo dyes [20,23,24], a class of organic molecules widely applied in photographic and textile industries, generating a negative impact once released in the environment [25,26]. Different methods have been proposed for azo-dye removal from the environment, including adsorption [27,28], reduction by nanoscale zerovalent iron [25,29], and photocatalytic degradation with TiO_2 [25], generally in the presence of an oxidizing agent, such as H_2O_2 [23,30].

From a photocatalytic point of view, doping TiO_2 with heteroatoms extends its absorption towards the Vis range and enhances the stabilization of electron/hole pairs usually characterized by a short life-time [11,31–33]. The doping method is of paramount importance in determining the UV-Vis absorption properties and the photocatalytic activity of the final material: different means of TiO_2 doping have been investigated so far, mainly by the use of transition metals (V, Fe, Ag, Co and Cu) [22,23,31,34–36], but also non-metals, such as carbon [11] or nitrogen [37,38]. The interest for N-doping has spread in the last decade, as $\text{TiO}_{2-x}\text{N}_x$ nanoparticles showed superior photocatalytic performances with respect to commercial Degussa P25 (hereafter referred to as P25) [39].

In the present paper, nanoparticles (NPs) of mesoporous TiO_2 (MT) were prepared and Fe was added by either direct synthesis doping or impregnation: as a dopant, Fe extends TiO_2 absorption towards the Vis range, may enhance the separation of photo-generated electrons/holes and increases absorption in the UV region [40–42].

In this manuscript, the following samples were considered: pure mesoporous TiO_2 (MT); the same impregnated with 2.5 wt.% Fe (Fe2.5-MTi); Fe-doped MT prepared by direct synthesis with 2.5 wt.% Fe (Fe2.5-MTd); P25 [43] and the same impregnated with either 0.80 or 2.5 wt.% Fe (Fe0.80-IT and Fe2.5-IT).

The MT sample was prepared by a soft-template method to be compared to P25, the commercial TiO_2 reported in most literature papers: calcination of MT was carried out at 450 °C, a temperature allowing template removal along with formation of pure anatase, the TiO_2 polymorph characterized by remarkable SSA and superior photocatalytic performance in the UV range [14].

Fe containing samples were prepared with the aims of comparing direct synthesis (Fe2.5-MTd) to impregnation (Fe2.5-MTi, Fe0.80-IT and Fe2.5-IT) and of discriminating between the behavior of Fe species in the bulk and/or at the surface.

Two nominal concentrations of Fe were considered for impregnation of P25, namely 0.80 and 2.5 wt.%, in order to consider the effect of Fe dispersion on P25 ($\text{SSA} = 56 \text{ m}^2 \cdot \text{g}^{-1}$, *vide infra*) and on MT ($\text{SSA} = 150 \text{ m}^2 \cdot \text{g}^{-1}$, i.e., three-fold that of P25).

The degradation of Acid Orange 7 (AO7) (a model azo dye) was studied in different experimental conditions. In dark conditions, the redox chemistry of surface species was addressed and the effect of the oxidation state of surface Fe species was studied by incubating Fe2.5-MTd sample with ascorbic acid, a mild reducing agent, in order to produce surface Fe^{2+} species, which are more reactive in the Fenton process with respect to Fe^{3+} species [24,30,44]; the effect of H_2O_2 concentration (that can affect dye conversion) was also considered. Photocatalytic tests under UV illumination, allowed investigation of the effect of Fe doping as well as comparing our samples with commercial P25. Finally, under simulated solar light, the catalysts were studied under desirable conditions for future water remediation processes.

2. Results

2.1. Relevant Physico-Chemical Properties of the Prepared Samples

X-ray diffraction patterns (XRD) of MT and P25 are reported in Figure 1a, along with the corresponding Rietveld refinements: in MT the only phase present was anatase (99.8 wt.%), whereas, as expected, a mixture of anatase (88.8 wt.%) and rutile (11.2 wt.%) was found in P25. The crystallite size of MT was about 15 nm, as calculated through the Debye-Scherrer formula (Table 1), in agreement with FESEM (Field Emission Scanning Electron Microscopy) images (Figure 1b,c), which revealed a homogenous morphology of NPs with the MT sample, at variance with P25 showing larger and more irregular particles.

N₂ adsorption/desorption isotherms at −196 °C (not reported) on MT samples were Type IV, showing the occurrence of both intra- and inter-particles mesopores. The corresponding values of SSA (Table 1) were much higher than P25 samples. Interestingly, the SSA of the Fe2.5-MTd sample (where Fe doping was obtained by direct synthesis) was almost unaffected by Fe doping, whereas a sizeable decrease of SSA occurred with the Fe2.5-MTi sample, probably due to the second annealing treatment following the impregnation and/or to some pores occlusion occurring during such a procedure.

Table 1. Textural properties of the studied samples as obtained by X-ray powders diffraction, N₂ isotherms at −196 °C, Energy Dispersive X-ray (EDX) analysis and X-ray Photoelectron Spectroscopy (XPS).

Sample	Preparation	Crystallites Size (nm)	SSA (m ² ·g ^{−1}) ^a	Metal Content (wt.%) ^b	Surface Metal Content (wt.%) ^c	Metal Density (Atoms nm ^{−2}) ^d
MT	Soft-template synthesis	14 ± 3 (Anatase)	150	-	-	-
P25	Commercial	19 ± 3 (Anatase) 23 ± 4 (Rutile)	56	-	-	-
Fe2.5-MTd	Direct Synthesis	11 ± 3 (Anatase)	147	2.5	1.33 ± 0.20	1.8 (0.97 °)
IFe0.8-IT	Impregnation of P25	21 ± 4 (Anatase) 28 ± 2 (Rutile)	56	0.80	1.10 ± 0.20	1.5 (2.1 °)
Fe2.5-MTi	Impregnation of MT	11 ± 1 (Anatase)	106	2.6	2.30 ± 0.20	2.7 (2.4 °)
Fe2.5-IT	Impregnation of P25	-	50	2.8	-	6.0

^a Specific Surface Area (SSA) as obtained by applying the Brunauer-Emmett-Teller (BET) method; ^b as determined by EDX analysis; ^c as determined by XPS analysis; ^d as calculated by applying the formula $[M/(SSA \cdot AM)] \cdot N_A$ where M is the metal-content (wt.%), SSA is the BET SSA, AM is the atomic mass of Fe and N_A is Avogadro's Number.

Figure 1d reports the DR-UV-Vis spectra of both MT and P25 samples, previously outgassed at 150 °C to remove water and other atmospheric contaminants. MT absorbs in a broader range of wavelengths with respect to P25, as onset of absorption occurs at 400 nm and 375 nm with MT and P25, respectively, indicating a red-shift of the absorption band with the former. Accordingly, band-gap values obtained from the Tauc's plots in Figure 1f were 3.2 eV for P25, in agreement with the literature, and slightly lower (3.1 eV) for MT, likely due to different optical properties of the mesoporous material [45].

Differences in the DR-UV-Vis spectra of Fe doped samples were observed especially in the UV region (Figure 1e): with Fe2.5-MTd sample, at 275 nm a very intense charge transfer (CT) transition from 2p O^{2−} to 3d Fe³⁺ superposed the UV absorption of anatase, due to the fraction of Fe³⁺ cations entering the TiO₂ bulk. Accordingly, the measured band-gap was 3.0 eV, as shown by the corresponding Tauc's plot in Figure 1f. Absorption bands above 400 nm were due to the d-d transition of the Fe³⁺ species in Fe oxo-hydroxide clusters of increasing size, which was particularly evident with the sample Fe2.5-IT obtained by impregnation of P25, indicating the likely formation of larger Fe oxo-hydroxide clusters, in the latter.

XPS analysis on the sample Fe2.5-MTd, reported elsewhere [23], showed two lines at ca. 710.6 and 723 eV, attributed to 2p_{3/2} and 2p_{1/2} lines of the Fe³⁺ species, respectively. The XP-spectra obtained with the impregnated samples (curves not reported) did not allow us to carry out a detailed analysis of the speciation of Fe, since the lines of Fe²⁺ and Fe³⁺ were very close and the curve-fitting procedure may be strongly affected by the presence of satellite peaks, as reported by the literature [46–48]. However,

reduction of Fe^{3+} to Fe^{2+} was very unlikely in the adopted synthesis conditions, since the impregnation procedure was followed by calcination in air (as reported in the *Materials* section).

The calculated metal density defined as “number of Fe atoms per nm^2 ” is reported in Table 1, by considering data from both EDX microanalysis and XPS. According to EDX, Fe2.5-MTd and Fe0.80-IT showed similar metal densities, whereas Fe2.5-IT had a higher metal density due to the (lower) SSA of P25 (Table 1). In agreement with UV-Vis spectroscopy showing that part of Fe entered the TiO_2 bulk of Fe2.5-MTd sample, the amount of surface Fe in the sample prepared by direct synthesis (as determined by XPS) was only 1.3 wt.%, i.e., much lower as compared to the overall amount determined by EDX microanalysis (2.5 wt.%). This result also allowed for estimation (as EDX is generally a semi-quantitative technique) of how much Fe actually entered the bulk of MT by direct synthesis, and so it could be assumed that, by means of the adopted soft-template synthesis and with a nominal Fe content of 2.5 wt.%, ca. half of Fe entered the bulk. XPS quantitative analysis of Fe2.5-IT, instead, did not allow us to reliably quantify the concentration of surface Fe species, since the resultant sample was very heterogeneous, due to the presence of large Fe oxo-hydroxide aggregates, along with patches where Fe was not detectable at the surface.

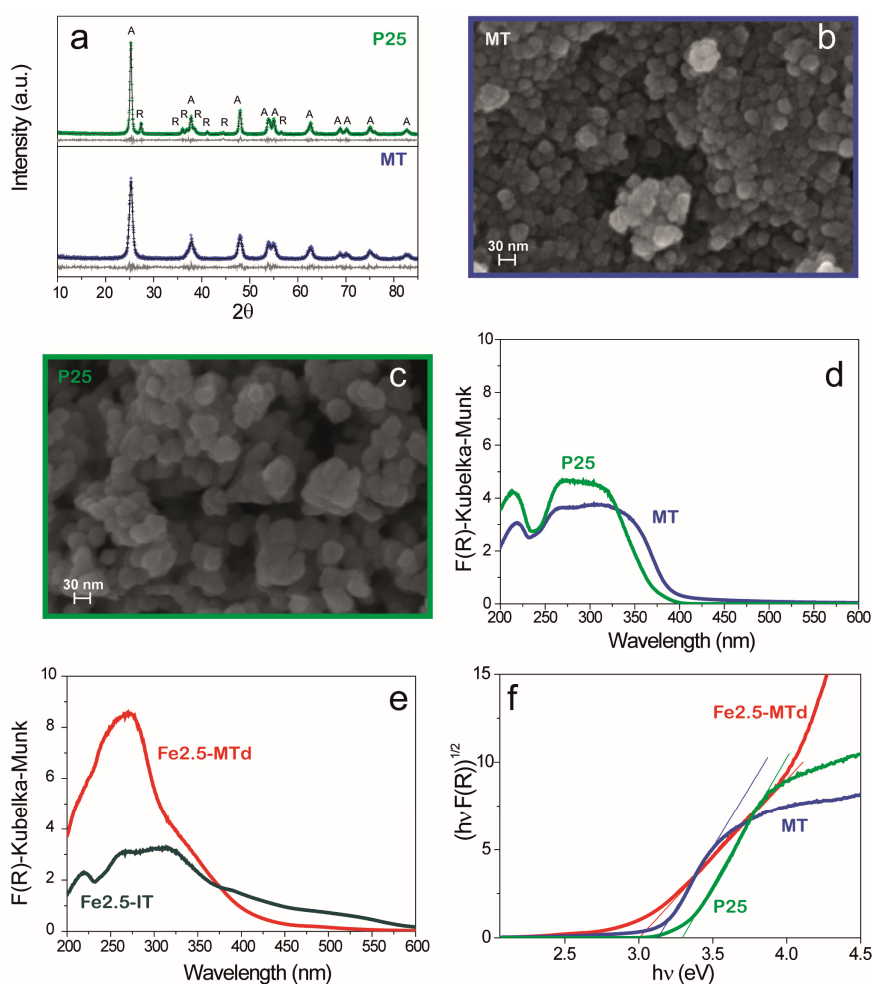


Figure 1. (a) XRD patterns and corresponding Rietveld refinements of mesoporous TiO_2 (MT) (experimental data, dark blue curve) and P25 (experimental data, green curve); grey curves correspond to the difference between experimental data and Rietveld refinements. A and R stand for anatase and rutile phase, respectively. (b) FESEM image of MT sample. (c) FESEM image of P25 sample. (d) DR-UV-Vis spectra of samples MT (blue curve) and P25 (green curve). (e) DR-UV-Vis spectra of samples Fe2.5-IT (dark green curve) and Fe2.5-MTd (red curve). (f) Tauc's plot of samples MT (blue curve), P25 (green curve) and Fe2.5-MTd (red curve).

2.2. AO7 Degradation Tests: Preliminary Considerations

Figure 2a reports the UV-Vis spectrum (orange curve) of the starting water solution used for degradation tests (0.67 mM, pH = 6.80), where two tautomer structures of AO7 occur (scheme). AO7 is a water-soluble dye with a hydroxyl group in the ortho-position to the azo group [25,26]. The hydrazone form, stable in the solid phase, in water undergoes an azo-hydrazone tautomerism via an intra-molecular proton transfer with the formation of two tautomer forms that are simultaneously present due to the acid-base equilibrium depicted in the scheme [26]. The spectrum of 0.67 mM AO7 showed two peaks at 310 and 230 nm, with a shoulder at 256 nm, due to absorption of aromatic rings. The peak at 484 nm (used to determine the amount of residual AO7 in solution and, consequently, to calculate the AO7 conversion percentage reported in the following) was related to the $n-\pi^*$ transition, which involves the lone pair of N atoms and the conjugated system extending over the two aromatic moieties and encompassing the N-N group of the hydrazone form [26,49]. The shoulder at 403 nm had a similar origin, involving, in this case, the N-N group of the azo form [26].

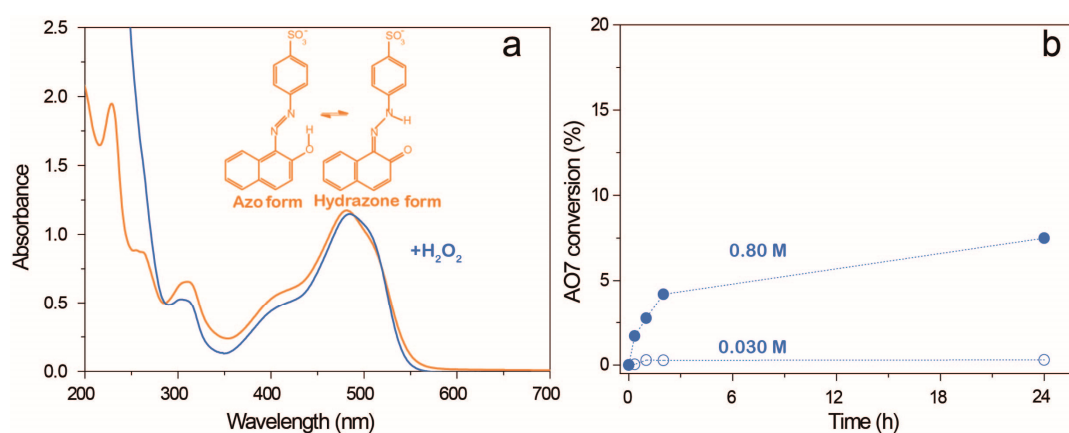


Figure 2. (a) UV-vis spectrum of the starting 0.67 mM AO7 aqueous solution (orange curve) and UV-vis spectrum obtained in a blank experiment (blue curve) carried out without catalyst by waiting 90 min after addition of 0.80 M H₂O₂; scheme of the azo-hydrazone tautomerism of AO7 in water. (b) Conversion percentage of AO7 as measured in dark conditions during blank experiments without any catalyst, in the presence of a stoichiometric amount of H₂O₂ (0.030 M, hollow symbols) and of an excess of H₂O₂ (0.80 M full symbols).

AO7 conversions obtained in blank experiments run in the absence of catalysts with either a stoichiometric amount or an excess amount of H₂O₂ (0.030 M and 0.80 M, respectively) were reported in Figure 2b. It was shown that H₂O₂ alone was poorly effective towards AO7 degradation, since a stoichiometric amount of H₂O₂ did not lead to appreciable dye conversion, whereas with excess H₂O₂, ca. 7.5% conversion was reached after 24 h, due to the generation of OH· radicals by H₂O₂ decomposition [50–52].

2.3. AO7 Degradation Tests: Catalytic Behavior of the Samples in Dark Conditions

The experiments were run at pH = 6.80, i.e., the natural pH of 0.67 mM AO7 solution, to avoid any competing adsorption phenomena: adsorption of AO7 at the surface of the solids was previously studied in the absence of H₂O₂ at different pH values [23]. It was shown that at pH = 6.80, the dye did not adsorb at the surface of the catalyst, whereas it did so at acidic pH values (2.20), at which the surface of TiO₂ was protonated and able to interact with AO7 anions.

Figure 3a,b report UV-Vis spectra concerning the experiments in which the (starting) 0.67 mM AO7 solution was in contact with the catalysts and 0.030 M H₂O₂ under dark conditions; Figure 3c,d report the results concerning similar experiments carried out with 0.80 M H₂O₂. Independent of the H₂O₂ concentration, the AO7 bands decreased in intensity, while no new band, ascribable to

any decomposition product, was observed in the UV range. It was noticed, however, that at higher H_2O_2 concentration, H_2O_2 absorption (blue curve in Figure 2a) dominated the region below 300 nm, inhibiting the spectroscopic detection of possible by-products absorbing in this region. Moreover, 0.80 M concentration provided H_2O_2 in excess and the intensity of the band absorbing below 340 nm remained unchanged during this time.

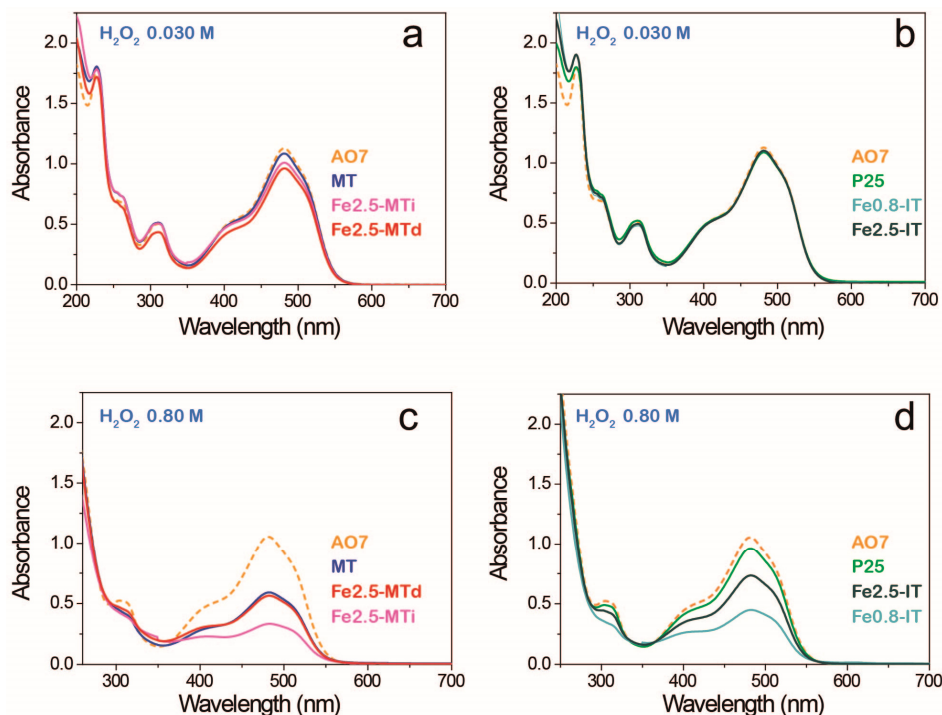


Figure 3. UV-Vis spectra of the (supernatant) solutions obtained after 24 h under dark conditions in the presence of H_2O_2 and the catalysts (dotted line: starting 0.67 mM AO7 solution). (a) UV-Vis spectra concerning experiments carried out with 0.030 M of H_2O_2 and MT samples. (b) UV-Vis spectra concerning experiments carried out with 0.030 M of H_2O_2 and P25 samples. (c) UV-Vis spectra concerning experiments carried out with 0.80 M H_2O_2 and MT samples. (d) UV-Vis spectra concerning experiments carried out with 0.80 M of H_2O_2 and P25 samples.

Figure 3a,b show that, under dark conditions, a stoichiometric amount of H_2O_2 was unable to promote any relevant AO7 conversion, as the degradation of AO7 was negligible after 24 h, even in the presence of the catalysts. On the contrary, AO7 conversion was higher with 0.80 M H_2O_2 , especially with Fe-containing catalysts (Figure 3c,d). Interestingly, bare MT showed a higher conversion than P25, probably due its higher SSA, and Fe-impregnated samples (independently on the support) showed better conversion than Fe2.5-MTd, in agreement with a lower surface metal density as determined by XPS (Table 1). This latter result showed that Fe^{3+} species at the surface of the catalysts were active under dark conditions, as they likely reacted with H_2O_2 through a Fenton-like mechanism (*vide infra*).

Table 2 shows that, as expected, the final conversion (i.e., the percentage of AO7 conversion after 96 h under dark conditions) increased with H_2O_2 concentration, especially with samples Fe2.5-MTd, Fe0.8-IT, and Fe2.5-MTi, where Fe was better dispersed with respect to Fe2.5-IT. Though the measurement of the initial rate (within the first 20 min of the reaction) was more affected by error than the final conversion, the positive effect of excess H_2O_2 on the initial conversion rate was less evident. This was likely due to the fact that a high concentration of H_2O_2 can scavenge $HO\cdot$ radicals with formation of $HO_2\cdot$ radicals [Equation (1)] with a lower oxidation power, which may slow down AO7 degradation:

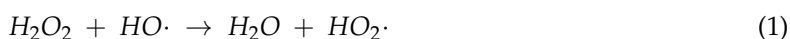


Table 2. Initial velocity ($M \cdot s^{-1}$) in the first 20 min and final conversion after 96 h, as obtained under dark conditions with 0.030 M and 0.80 M H_2O_2 .

Sample	Initial Rate with 0.030 M H_2O_2 ($M \cdot s^{-1} \cdot 10^{-8}$)	Final Conversion with 0.030 M H_2O_2 (%)	Initial Rate with 0.80 M H_2O_2 ($M \cdot s^{-1} \cdot 10^{-8}$)	Final Conversion with 0.80 M H_2O_2 (%)
MT	3.1	9	5.8	66
P25	2.7	5.2	1.0	25
Fe2.5-MTd	3.1	27	4.2	90
Fe0.8-IT	2.3	9.6	2.4	98
Fe2.5-MTi	5.6	31	17	100
Fe2.5-IT	2.1	7.8	1.0	79

Figure 4 reports the comparison of the conversion vs. time curves under dark conditions for the studied catalysts. Concerning the supports, MT exhibited ca. double conversion values compared to P25 during the studied time range, probably due to the higher SSA of the former sample. The reactivity of TiO_2 with H_2O_2 involves the formation of Ti-O-O-H (peroxo) bridges [53]. In the presence of H_2O_2 , part of the surface Ti-OH groups reacts with H_2O_2 by forming Ti-OOH species, more reactive than H_2O_2 in partial oxidation reactions [20,23]. The formation of such surface Ti-OOH species was already revealed by XPS [23], showing more abundant Ti-OOH species in MT than in P25, since the former material exhibits higher SSA.

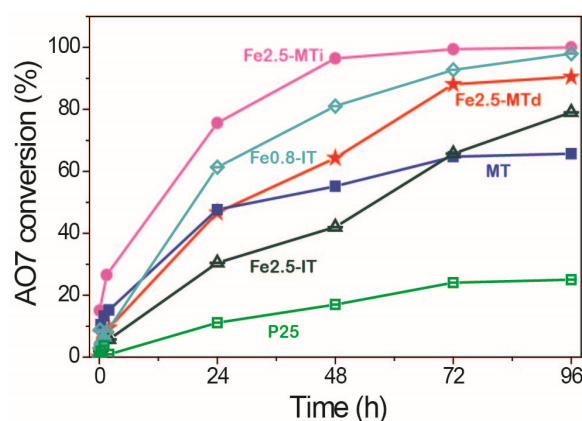


Figure 4. Catalytic activity in the degradation of AO7 reported as percentage of AO7 conversion versus time (h) (Dark conditions; H_2O_2 concentration: 0–80 M; catalyst concentration: $1.0 \text{ g} \cdot \text{L}^{-1}$).

Fe-containing samples were more active than the mere supports, with the exception of Fe2.5-IT that in the first 72 h was less active than the MT sample. Fe2.5-MTi sample, where the best compromise was obtained between surface Fe content and SSA, was the most active catalyst under dark conditions. The latter sample also showed the fastest initial rate and highest AO7 conversion, likely due to a better Fe dispersion obtained by impregnating MT with respect to P25. The metal density of Fe2.5-MTi with respect to Fe2.5-MTd (Table 1) explained the higher conversion obtained with the former under dark conditions, in which the redox reactivity of Fe species in the presence of H_2O_2 is exploited.

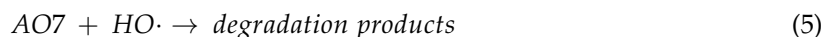
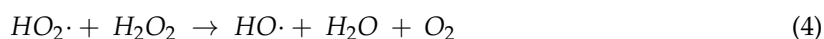
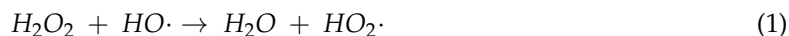
The shape of the conversion curves obtained with Fe2.5-MTd and MT samples is similar (Figure 4), and during the first 24 h the two curves nearly coincided. On the one side, the TiO_2 surface was active *per se* towards the degradation of the dye (*vide supra*) and, on the other side, the amount of active Fe^{3+} species at the surface of Fe2.5-MTd was lower (Table 1). It has to be considered, however, that a different coordination of surface Fe^{3+} species could be obtained by direct synthesis with respect to impregnation, as well. In fact, with Fe2.5-MTd, in dark conditions, surface Fe^{3+} ions started to promote AO7 conversion at a later stage.

Concerning the redox chemistry of Fe-doped samples, a Fenton-like mechanism [54] was inferred, which may occur both in homogeneous phase (i.e., aqueous solution) and with heterogeneous catalysts,

as well [30,55,56]. Though both Fe^{2+} and Fe^{3+} ions may react with H_2O_2 to form radicals [30,57], the latter react more slowly, according to the following reactions:



followed by



According to Pignatello et al. [44], Reaction (2) is several orders of magnitude slower than Reaction (3), and become the rate determining step: starting from Fe^{3+} species often results in a slower initial rate (or even a lag phase), especially with aromatic contaminants. The slowness of Reaction (2) explains the substantial lag of time for the onset of the Fenton reaction catalysed by Fe species. Due to the different rate of Reactions (2) and (3), the initial concentration of Fe^{2+} species at the catalyst surface is expected to be negligible (*vide supra*).

In order to confirm this hypothesis, the absence of Fe^{2+} species was checked by Mössbauer spectroscopy with Fe2.5-MTd sample (Figure 5): similar to previous reports of Fe-doped TiO_2 materials [58–60].

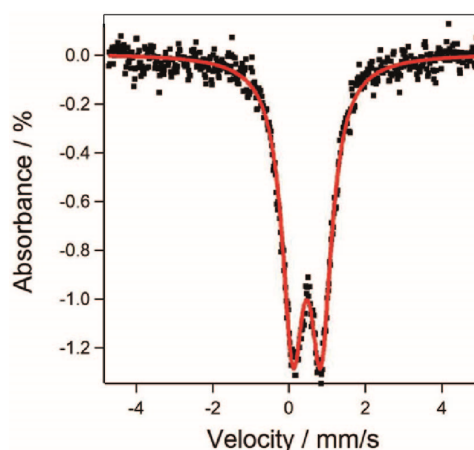


Figure 5. Zero-field ^{57}Fe Mössbauer spectrum of Fe2.5-MTd sample at $-183\text{ }^\circ\text{C}$: Solid red line represents the fit to the data and yields the following parameters: $\delta = 0.47\text{ mm/s}$; $|\Delta E_Q| = 0.73\text{ mm/s}$.

Since surface Fe^{2+} species would undergo a faster Fenton reaction, Fe2.5-MTd sample was incubated for 20 min with ascorbic acid (AA). The latter molecule is a (mild) reducing agent of metal ions and/or organic moieties, as well as a radical scavenger. Figure 6 reports the UV-Vis spectra recorded after incubating the Fe2.5-MTd sample with an amount of AA corresponding to the number of moles of H_2O_2 able to react with AO7 in stoichiometric conditions (according to Equation (12), i.e., $0.030\text{ M H}_2\text{O}_2$). The catalytic activity of the sample in dark conditions significantly increased (Figure 6), and the dye was almost completely degraded after 5 min. The main evidence in Figure 6 was that AA boosted the Fenton reaction by continuously reducing Fe^{3+} species to Fe^{2+} : by this way, the Reaction (3) was favored on Reaction (2). After adding H_2O_2 , two minor bands (asterisks) form, which can be ascribed to *o*-naphthoquinone: the presence of this moiety was not surprising, and according to the literature, is a by-product of AO7 degradation formed by side-reactions occurring during both reduction and oxidation of the dye [25].

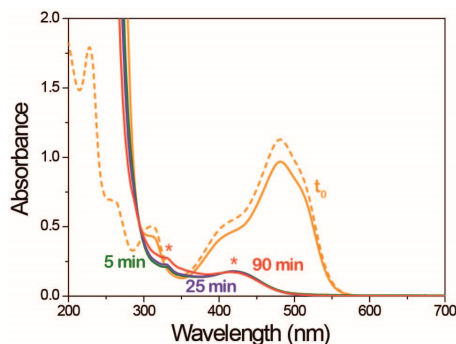


Figure 6. UV-Vis spectra of AO7 solution (dotted orange line) in dark conditions in presence of Fe2.5-MTd that was pre-incubated for 20 min with 0.030 M AA (t_0 curve, solid orange curve). After adding 0.03 M H_2O_2 , supernatant solutions were collected after 5 min (green curve), 25 min (purple curve) and 90 min (red curve).

Summarizing, Fe-containing samples showed a high activity towards AO7 degradation under dark conditions, with the exception of the Fe2.5-IT sample, where poor Fe dispersion can play a detrimental role due to the formation of less active Fe oxo-hydride aggregates. Moreover, being the surface density of Fe low, active patches of TiO_2 were still available at the surface of Fe-containing samples, where both TiO_2 patches and Fe species contributed to the dye conversion.

2.4. AO7 Degradation Tests under UV Irradiation

Photocatalytic results obtained after 20 min under illumination with 0.030 M H_2O_2 are reported in Figure 7 along with results concerning the following blank experiments: (i) UV photodegradation without any catalyst and (ii) UV photodegradation without H_2O_2 , with the aim of exploiting O_2 dissolved in water in the presence of the catalysts, as the solutions were not de-aerated. Figure 7 shows that without catalysts, the maximum conversion was ca. 20%, whereas in the absence of H_2O_2 the best performance (i.e., 37% conversion) was obtained with the Fe2.5-MTd sample, due to the positive effect of bulk Fe species (obtained by direct synthesis) that improve UV light absorption.

The addition of H_2O_2 to the reaction mixture promoted the photocatalytic activity of all of the samples, as expected. With the two supports, similar AO7 conversion was obtained; with bare TiO_2 , H_2O_2 most likely acted as an acceptor of photogenerated electrons (e^-):



According to Equation (6), hydroxyl radicals, active in the degradation of AO7, are produced.

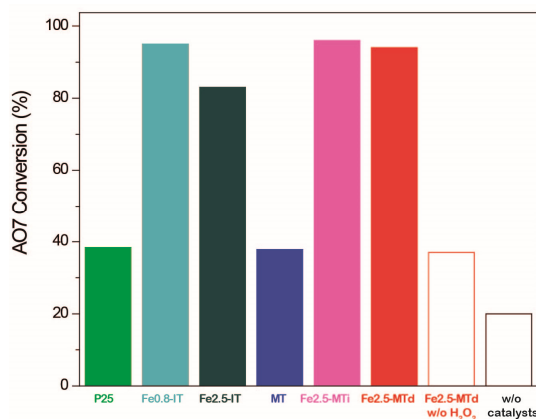
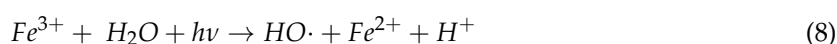
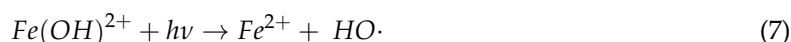


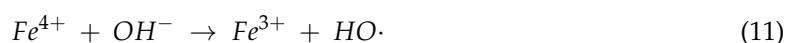
Figure 7. Histograms of AO7 conversion after 20 min under a UV lamp with 0.030 M H_2O_2 .

MT and P25 showed similar conversion, indicating that the positive effect of the higher SSA in MT was counterbalanced by the peculiar anatase/rutile composition of P25 that, according to the literature, efficiently stabilizes photogenerated electron/hole pairs [14,40,61].

With Fe-containing samples, AO7 degradation was almost complete, and the two samples characterized by the highest surface metal density (Fe2.5-MTi and Fe0.8-IT, Table 1) were the most active samples. Under UV irradiation, the so-called photo-assisted Fenton reaction (or photo-Fenton system) occurs [44], through which Fe^{2+} species are regenerated by photolysis of Fe^{3+} hydroxide complexes yielding additional HO· radicals [Equations (7) and (8)]; simultaneously, photocatalytic decomposition of H_2O_2 occurs [Equation (9)]:



Photogenerated holes probably react with Fe^{3+} species forming (unstable) Fe^{4+} species, which further react by producing HO· radicals, according to Equations (10) and (11):



2.5. AO7 Degradation Tests under Simulated Solar Light (1 SUN)

In order to test the samples in conditions exploitable for future development of efficient water remediation systems, their photocatalytic efficiency was tested under simulated solar light (Figure 8). Although AO7 moieties have a strong absorption cross section in the visible part of the solar spectrum, which can hinder the photocatalyst activation under Vis light, fair results were obtained, and the best performance, with ~56% of conversion, was achieved by the Fe2.5-MTd sample, which had the strongest absorption in the UV region and the smallest band gap (Figure 1e,f). Besides the Fe species present in the bulk (strongly absorbing in the 250–300 nm range, with a maximum at 275 nm), Fe species were also fairly distributed at the surface, and may have rendered the catalyst able to absorb more photons at wavelengths below 400 nm, where AO7 absorption was weaker than in the visible range (Figure 2a). This phenomenon can promote the photogeneration of electron/hole pairs that react with the contaminant. The samples obtained by Fe impregnation showed instead a lower degradation conversion ability due to their lower absorption in the UV region, as compared to the sample obtained by direct synthesis. Under solar light, the two supports had similar behavior, although the P25 showed a slightly better performance.

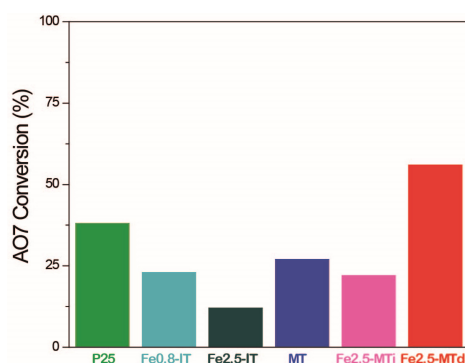


Figure 8. Histograms of AO7 conversion after 120 min under 1 SUN and in presence of 0.030 M H_2O_2 .

3. Discussion

Under dark conditions, MT showed higher activity than P25 during AO7 degradation, probably in virtue of its higher SSA, and therefore formation of reactive Ti-OOH species in the presence of H₂O₂ was favored.

The amount of well-dispersed surface Fe species had a crucial role during the reaction under dark conditions, and therefore the sample obtained by impregnating MT was the most active. Out of the two Fe-containing samples obtained by impregnation of P25, Fe0.8-IT provided better performance, corresponding to a lower Fe surface density and, consequently, to a better Fe dispersion. Under dark conditions, surface Fe species were involved in a Fenton-like reaction, when iron was present as Fe³⁺ species. Fe²⁺ species (more active in the Fenton process than Fe³⁺ species) formed upon incubation with ascorbic acid, essentially acting as a metal reducing agent in the adopted experimental conditions. The largest surface area of MT could be very useful for other reactions in dark conditions, as it significantly improves the contact with the contaminant and facilitates the dispersion of Fe species, active in Fenton-like processes. For instance, in view of an actual application of the photo-Fenton method to wastewater treatment, homogeneous catalysts bring some limitations, due to the production of Fe-containing sludge, catalyst deactivation and the limited range of operating pH [62], whereas the studied catalysts were active at the natural pH of the solution. Several studies have been also carried out on heterogeneous photo-Fenton systems implying, for instance, the oxidation of AO7 by Fe-bentonite and Fe-laponite catalysts [63].

Under UV illumination, notwithstanding the higher specific surface area, the activity of MT was comparable to that of P25: as recognized by the literature, the peculiar anatase/rutile mixture occurring in the commercial material allowed superior photocatalytic performance, due to the stabilization of electron/hole pairs. Future work will concern attempts to improve the photocatalytic activity of MT, by following alternative synthesis procedures as well as different thermal treatments. The former could help to obtain smaller nanoparticles, and the latter could be adopted to obtain different polymorphs (or mixtures of polymorphs) trying to mimic the composition of P25, still maintaining the higher SSA typical of materials obtained by soft-template synthesis.

The behavior of the Fe2.5-MTd sample under UV illumination showed that Fe³⁺ species in the bulk (absorbing at 275 nm) are able to enhance the photocatalytic activity of MT: this effect is confirmed in the absence of H₂O₂ as the sample showed the highest activity in blank experiments without addition of hydrogen peroxide. Moreover, the Fe2.5-MTd sample was also the most active one under simulated solar light, when it was able to exploit the UV fraction of the solar spectrum (ca. 2% in the used simulator) more efficiently than the other samples studied. "Direct synthesis" allows a partial introduction of Fe in the bulk of MT, with a consequent improvement in photocatalytic activity of Fe2.5-MTd with respect to MT, whereas surface Fe species are able to undergo a photo-Fenton process in the presence of H₂O₂. Under UV light, impregnated samples were also very active in the presence of H₂O₂: this was likely due to the fact that all Fe³⁺ species were at the surface and therefore available to accept both photogenerated electrons, forming (more reactive) Fe²⁺ species, and photogenerated holes, forming very reactive Fe⁴⁺ species [40] [Equation (10)]. In fact, the samples prepared by impregnation showed similar activity (independent of the support) due to the UV-induced processes mentioned previously.

In summary, the catalytic and photocatalytic behavior of the samples was studied under very different reaction conditions, i.e., dark, UV light, and simulated solar light. The ensemble of such experiments, along with the physico-chemical characterization, allowed a thorough picture of the system to be formed, and allowed some positive effects of Fe-doping, as obtained by direct synthesis, to be characterised. Indeed, the catalyst prepared by direct synthesis showed the best performance under solar illumination, i.e., under experimental conditions that could be useful for future applications in water remediation, where solar light could be exploited to abate the costs of UV irradiation. Addition of a magnetic phase, as reported in the literature [64], could render this kind of materials even more attractive for practical usage, also guaranteeing a facile separation of the solids after their use.

4. Materials and Methods

4.1. Materials

ACS (American Chemical Society) grade chemicals from Sigma-Aldrich (Milan, Italy) were used as reagents.

The sample of mesoporous titania (MT) was obtained by soft-template synthesis as reported in [20] and [23]. Two solutions were prepared: to obtain solution A, 5.0 g Ti(OBut)₄ (titanium *tert*-butoxide) were added dropwise to 30.0 mL acetic acid solution (20%, *v/v*) and the mixture was then vigorously stirred for about 4 h; to obtain solution B, 3.0 g Pluronic P123 and ca. 20.0 mL ethanol were mixed. Solution B was then dropwise added to solution A: the resulting mixture was sealed, stirred for 24 h at room temperature and transferred into a Teflon autoclave for hydrothermal treatment at 95 °C for 48 h. The resulting precipitate was centrifuged, dried at 80 °C and calcined in air at 450 °C for 4 h.

Fe-containing MT with 2.5 wt.% nominal Fe content (Fe2.5-MTd) was prepared by adding 0.25 g FeCl₃·6H₂O to solution A, which was sealed and stirred for 4 h; solution B was then dropwise added to solution A and the resulting mixture was stirred for 24 h at room temperature and treated at 95 °C for 48 h inside a Teflon autoclave. The resulting precipitate was filtered, dried at 60 °C and calcined in air at 450 °C for 4 h.

Similarly, Fe-containing MT and commercial Degussa P25 (TiO₂ content ≥ 99.5%), with comparable nominal Fe contents (ca. 0.8–2.5 wt.%) were obtained by impregnation of MT (Fe2.5-MTi) and P25 (Fe0.80-IT and Fe2.5-IT) with a aqueous solution of FeCl₃·6H₂O, followed by drying at 60 °C and calcination in air at 450 °C for 4 h. This procedure in the manuscript is referred to as an “impregnation method”.

4.2. Methods

Powder X-ray diffraction patterns were collected on a X'Pert Philips PW3040 diffractometer (PANalytical, Almelo, The Netherlands) using Cu K α radiation (2θ range = 20°–85°; step = 0.05° 2 θ ; time per step = 0.2 s), and were indexed according to the Powder Data File database (PDF 2000, International Centre of Diffraction Data, Newtown Square, PA, USA). Crystallites average size (D) was determined by using the Debye-Scherrer formula $D = 0.9 \lambda / b \cdot \cos\theta$, where λ is the wavelength of the Cu K α radiation, b is the full width at half maximum (in radians), 0.9 is the shape factor for spherical particles and θ is the angle of diffraction peaks. The full-profile Rietveld method applied to diffraction patterns using the GSAS-EXPGUI free software was used to evaluate the anatase content. XRD background was modeled by a 10-term cosine polynomial function, and pseudo-Voigt functions were adopted for curve fitting.

Specific Surface Area (SSA) were measured by N₂ physisorption at –196 °C (Quantachrome Autosorb 1C, Boyton Beach, FL, USA) on powders outgassed at 150 °C for 4 h to remove water and other atmospheric contaminants; SSA was determined according to the Brunauer-Emmett-Teller (BET) method.

Diffuse Reflectance (DR) UV-Vis spectra of powder samples dehydrated at 150 °C were measured on a Cary 5000 UV-Vis-NIR spectrophotometer (Varian Instruments, Mulgrave, Australia) equipped with a DR apparatus.

The metal content was determined by (semi-quantitative) chemical analysis carried out by means of an Energy Dispersive X-ray (EDX) probe (low vacuum Scanning Electron Microscope Quanta inspect 200, FEI, Hillsboro, OR, USA) on 10–50 nm diameter spots. For each sample, about 10 measurements were carried out in different spots of the sample, from which an average metal content was calculated, as reported in Table 1.

X-ray Photoelectron Spectroscopy (XPS) analyses were run on a PHI 5000 Versa Probe II Scanning XPS Microprobe spectrometer (ULVAC-PHI Inc., Kanagawa, Japan). The measurements were done with a monochromatised Al K α source (X-ray spot 100 μ m), at a power of 24.8 W. Wide scans and detailed spectra were acquired in Fixed Analyzer Transmission (FAT) mode with a pass energy of

117.40 eV and 46.95 eV, respectively. An electron gun was used for charge compensation (1.0 V 20.0 μ A). Data processing was performed by using the MultiPak software v. 9.5.0.8.

The zero-field ^{57}Fe Mössbauer spectrum of Fe-MT sample was measured with a constant acceleration spectrometer (SEE Co., Minneapolis, MN, USA). The Fe2.5-MTd sample (ca. 50 mg) was prepared as a Paratone-N mull and frozen in liquid nitrogen prior to insertion into the spectrometer. Isomer shifts are quoted relative to Fe metal at 23 °C. Data was acquired at -183 °C and processed, simulated, and analyzed using an in-house package for IGOR Pro 6 (Wavemetrics, Lake Oswego, OR, USA).

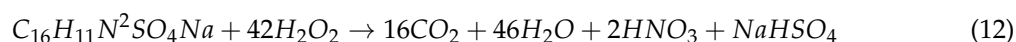
4.3. Catalytic Tests

Catalytic tests were carried out systematically adding an amount of catalyst corresponding to $1.0 \text{ g}\cdot\text{L}^{-1}$ concentration to 50 mL of 0.67 mM aqueous solution (natural pH = 6.8) of AO7 (Fluka) and. Preliminary blank experiments were run under dark conditions by (i) mixing 0.67 mM AO7 with either 0.030 M or 0.80 M H_2O_2 without any catalyst and by (ii) mixing 0.67 mM AO7 with $1.0 \text{ g}\cdot\text{L}^{-1}$ catalyst in the absence of H_2O_2 .

A first set of experiments was carried out in dark conditions by adding either 0.030 M or 0.80 M H_2O_2 to the suspension containing AO7 and the solid. A second set was performed under UV light with 0.030 M H_2O_2 by illuminating with a medium-pressure Hg lamp (-; light intensity of $55 \text{ mW}\cdot\text{cm}^{-2}$, LC3, Hamamatsu Photonic, Hamamatsu, Japan). A third set was performed with 0.030 M H_2O_2 under illumination by simulated solar light (AM 1.5 G, $100 \text{ mW}\cdot\text{cm}^{-2}$) obtained through a plasma lamp (LIFI STA-40, LUXIM, Santa Clara, CA, USA). 1 SUN: $\sim 1000 \text{ W}\cdot\text{m}^{-2}$ in the visible range and $\sim 22 \text{ W}\cdot\text{m}^{-2}$ in the UV range, corresponding to ca. 4% of the power of the UV lamp used in the second set of experiments).

In all cases, the suspension was continuously stirred by means of a magnetic stirrer, operated at 300 rpm. Since the reaction mixture was not de-aerated, atmospheric O_2 was always present.

Concerning the amount of H_2O_2 used during tests, let us consider the reaction leading to the complete degradation of the dye:



Equation (12) shows that a 0.030 M H_2O_2 concentration roughly corresponds to the stoichiometric amount of H_2O_2 necessary for complete AO7 degradation.

During catalytic tests, several aliquots of the suspension were collected at regular intervals of time. The supernatant fraction was separated by centrifugation (ALC centrifuge PK110, at 4000 rpm for 2 min) and the UV-Vis spectrum was measured by means of a Cary 5000 UV-Vis-NIR spectrophotometer (Varian Instruments, Mulgrave, Australia), using a quartz cell with 1 mm path length in the 190–800 nm range. After a calibration procedure, the AO7 concentration was calculated by the intensity of its 484 nm band.

Acknowledgments: The authors thank Fondazione Cariplo (Italy) for financial support through the grant 2015–0186 “DeN—Innovative technologies for the abatement of N-containing pollutants in water” (Principal Investigator: I. Rossetti). The authors thank Marco Sangermano (DISAT, Politecnico di Torino) for lending the UV lamp and Simelys Hernandez for lending the simulated solar light lamp; G. Menard (Department of Chemistry and Chemical Biology, Harvard University) for Mössbauer spectroscopy measurements and E. Garrone for fruitful discussion.

Author Contributions: F.S.F., B.B. and M.P. designed the experiments. N.D. run the XPS measurements and the related curve-fitting procedure. F.S.F. performed the other experiments along with M.P. and M.C., F.S.F. and B.B. wrote the manuscript. I.R. and G.R. critically revised the manuscript.

Conflicts of Interest: The authors declare no conflict of interest.

References

1. Ge, M.; Cao, C.; Huang, J.; Li, S.; Chen, Z.; Zhang, K.-Q.; Al-Deyab, S.S.; Lai, Y. A review of one-dimensional TiO₂ nanostructured materials for environmental and energy applications. *J. Mater. Chem. A* **2016**, *4*, 6772–6801. [[CrossRef](#)]
2. Liao, J.-Y.; He, J.-W.; Xu, H.; Kuang, D.-B.; Su, C.-Y. Effect of TiO₂ morphology on photovoltaic performance of dye-sensitized solar cells: Nanoparticles, nanofibers, hierarchical spheres and ellipsoid spheres. *J. Mater. Chem.* **2012**, *22*, 7910–7918. [[CrossRef](#)]
3. Nakata, K.; Fujishima, A. TiO₂ photocatalysis: Design and applications. *J. Photochem. Photobiol. C Photochem. Rev.* **2012**, *13*, 169–189. [[CrossRef](#)]
4. Zhang, R.; Elzatahry, A.A.; Al-Deyab, S.S.; Zhao, D. Mesoporous titania: From synthesis to application. *Nano Today* **2012**, *7*, 344–366. [[CrossRef](#)]
5. Zhou, X.; Liu, N.; Schmuki, P. Photocatalysis with TiO₂ Nanotubes: “Colorful” Reactivity and Designing Site-Specific Photocatalytic Centers into TiO₂ Nanotubes. *ACS Catal.* **2017**, *7*, 3210–3235. [[CrossRef](#)]
6. Schneider, J.; Matsuoka, M.; Takeuchi, M.; Zhang, J.; Horiuchi, Y.; Anpo, M.; Bahnemann, D.W. Understanding TiO₂ Photocatalysis: Mechanisms and Materials. *Chem. Rev.* **2014**, *114*, 9919–9986. [[CrossRef](#)] [[PubMed](#)]
7. Ma, Y.; Wang, X.; Jia, Y.; Chen, X.; Han, H.; Li, C. Titanium Dioxide-Based Nanomaterials for Photocatalytic Fuel Generations. *Chem. Rev.* **2014**, *114*, 9987–10043. [[CrossRef](#)] [[PubMed](#)]
8. Sauvage, F.; Chen, D.; Comte, P.; Huang, F.; Heiniger, L.-P.; Cheng, Y.-B.; Caruso, R.A.; Graetzel, M. Dye-Sensitized Solar Cells Employing a Single Film of Mesoporous TiO₂ Beads Achieve Power Conversion Efficiencies Over 10%. *ACS Nano* **2010**, *4*, 4420–4425. [[CrossRef](#)] [[PubMed](#)]
9. O’Regan, B.; Gratzel, M. A low-cost, high-efficiency solar cell based on dye-sensitized colloidal TiO₂ films. *Nature* **1991**, *353*, 737–740. [[CrossRef](#)]
10. Roose, B.; Pathak, S.; Steiner, U. Doping of TiO₂ for sensitized solar cells. *Chem. Soc. Rev.* **2015**, *44*, 8326–8349. [[CrossRef](#)] [[PubMed](#)]
11. Lin, A.; Qi, D.; Ding, H.; Wang, L.; Xing, M.; Shen, B.; Zhang, J. Carbon-doped titanium dioxide nanocrystals for highly efficient dye-sensitized solar cells. *Catal. Today* **2017**, *281*, 636–641. [[CrossRef](#)]
12. Rajh, T.; Dimitrijevic, N.M.; Bissonnette, M.; Koritarov, T.; Konda, V. Titanium Dioxide in the Service of the Biomedical Revolution. *Chem. Rev.* **2014**, *114*, 10177–10216. [[CrossRef](#)] [[PubMed](#)]
13. Wu, S.; Weng, Z.; Liu, X.; Yeung, K.W.K.; Chu, P.K. Functionalized TiO₂ Based Nanomaterials for Biomedical Applications. *Adv. Funct. Mater.* **2014**, *24*, 5464–5481. [[CrossRef](#)]
14. Bonelli, B.; Esposito, S.; Freyria, F.S. Mesoporous Titania: Synthesis, Properties and Comparison with Non-Porous Titania. In *Titanium Dioxide*; Janus, M., Ed.; Intech: Rijeka, Croatia, 2017.
15. Su, J.; Guo, L.; Bao, N.; Grimes, C.A. Nanostructured WO₃/BiVO₄ Heterojunction Films for Efficient Photoelectrochemical Water Splitting. *Nano Lett.* **2011**, *11*, 1928–1933. [[CrossRef](#)] [[PubMed](#)]
16. Li, R.; Weng, Y.; Zhou, X.; Wang, X.; Mi, Y.; Chong, R.; Han, H.; Li, C. Achieving overall water splitting using titanium dioxide-based photocatalysts of different phases. *Energy Environ. Sci.* **2015**, *8*, 2377–2382. [[CrossRef](#)]
17. Kou, J.; Lu, C.; Wang, J.; Chen, Y.; Xu, Z.; Varma, R.S. Selectivity Enhancement in Heterogeneous Photocatalytic Transformations. *Chem. Rev.* **2017**, *117*, 1445–1514. [[CrossRef](#)] [[PubMed](#)]
18. Lianos, P. Review of recent trends in photoelectrocatalytic conversion of solar energy to electricity and hydrogen. *Appl. Catal. B Environ.* **2017**, *210*, 235–254. [[CrossRef](#)]
19. Freyria, F.S.; Armandi, M.; Compagnoni, M.; Ramis, G.; Rossetti, I.; Bonelli, B. Catalytic and Photocatalytic Processes for the Abatement of N-Containing Pollutants From Wastewater. Part 2: Organic Pollutants. *J. Nanosci. Nanotechnol.* **2017**, *17*, 3654–3672. [[CrossRef](#)]
20. Piumetti, M.; Freyria, F.S.; Armandi, M.; Saracco, G.; Garrone, E.; Gonzalez, G.E.; Bonelli, B. Catalytic degradation of Acid Orange 7 by H₂O₂ as promoted by either bare or V-loaded titania under UV light, in dark conditions, and after incubating the catalysts in ascorbic acid. *Catal. Struct. React.* **2015**, *1*, 183–191. [[CrossRef](#)]
21. Khataee, A.R.; Kasiri, M.B. Photocatalytic degradation of organic dyes in the presence of nanostructured titanium dioxide: Influence of the chemical structure of dyes. *J. Mol. Catal. A Chem.* **2010**, *328*, 8–26. [[CrossRef](#)]
22. Rauf, M.A.; Meetani, M.A.; Hisaindee, S. An overview on the photocatalytic degradation of azo dyes in the presence of TiO₂ doped with selective transition metals. *Desalination* **2011**, *276*, 13–27. [[CrossRef](#)]

23. Piumetti, M.; Freyria, F.S.; Armandi, M.; Geobaldo, F.; Garrone, E.; Bonelli, B. Fe- and V-doped mesoporous titania prepared by direct synthesis: Characterization and role in the oxidation of AO7 by H₂O₂ in the dark. *Catal. Today* **2014**, *227*, 71–79. [[CrossRef](#)]
24. Piumetti, M.; Freyria, F.S.; Armandi, M.; Saracco, G.; Garrone, E.; Bonelli, B. Anti-oxidant/pro-oxidant activity of ascorbic acid. *Chem. Today* **2015**, *33*, 13–15.
25. Freyria, F.S.; Bonelli, B.; Sethi, R.; Armandi, M.; Belluso, E.; Garrone, E. Reactions of Acid Orange 7 with Iron Nanoparticles in Aqueous Solutions. *J. Phys. Chem. C* **2011**, *115*, 24143–24152. [[CrossRef](#)]
26. Momeni, S.; Nematollahi, D. New insights into the electrochemical behavior of acid orange 7: Convergent paired electrochemical synthesis of new aminonaphthol derivatives. *Sci. Rep.* **2017**, *7*. [[CrossRef](#)] [[PubMed](#)]
27. Shafia, E.; Esposito, S.; Armandi, M.; Bahadori, E.; Garrone, E.; Bonelli, B. Reactivity of bare and Fe-doped alumino-silicate nanotubes (imogolite) with H₂O₂ and the azo-dye Acid Orange 7. *Catal. Today* **2016**, *277*, 89–96. [[CrossRef](#)]
28. Sun, D.; Zhang, X.; Wu, Y.; Liu, X. Adsorption of anionic dyes from aqueous solution on fly ash. *J. Hazard. Mater.* **2010**, *181*, 335–342. [[CrossRef](#)] [[PubMed](#)]
29. Moon, B.H.; Park, Y.B.; Park, K.H. Fenton oxidation of Orange II by pre-reduction using nanoscale zero-valent iron. *Desalination* **2011**, *268*, 249–252. [[CrossRef](#)]
30. Ramirez, J.H.; Maldonado-Hódar, F.J.; Pérez-Cadenas, A.F.; Moreno-Castilla, C.; Costa, C.A.; Madeira, L.M. Azo-dye Orange II degradation by heterogeneous Fenton-like reaction using carbon-Fe catalysts. *Appl. Catal. B Environ.* **2007**, *75*, 312–323. [[CrossRef](#)]
31. Di Paola, A.; Marci, G.; Palmisano, L.; Schiavello, M.; Uosaki, K.; Ikeda, S.; Ohtani, B. Preparation of Polycrystalline TiO₂ Photocatalysts Impregnated with Various Transition Metal Ions: Characterization and Photocatalytic Activity for the Degradation of 4-Nitrophenol. *J. Phys. Chem. B* **2002**, *106*, 637–645. [[CrossRef](#)]
32. Pesci, F.M.; Wang, G.; Klug, D.R.; Li, Y.; Cowan, A.J. Efficient Suppression of Electron–Hole Recombination in Oxygen-Deficient Hydrogen-Treated TiO₂ Nanowires for Photoelectrochemical Water Splitting. *J. Phys. Chem. C* **2013**, *117*, 25837–25844. [[CrossRef](#)] [[PubMed](#)]
33. Sachs, M.; Pastor, E.; Kafizas, A.; Durrant, J.R. Evaluation of Surface State Mediated Charge Recombination in Anatase and Rutile TiO₂. *J. Phys. Chem. Lett.* **2016**, *7*, 3742–3746. [[CrossRef](#)] [[PubMed](#)]
34. Guayaquil-Sosa, J.F.; Serrano-Rosales, B.; Valadés-Pelayo, P.J.; de Lasa, H. Photocatalytic hydrogen production using mesoporous TiO₂ doped with Pt. *Appl. Catal. B Environ.* **2017**, *211*, 337–348. [[CrossRef](#)]
35. Ren, F.; Li, H.; Wang, Y.; Yang, J. Enhanced photocatalytic oxidation of propylene over V-doped TiO₂ photocatalyst: Reaction mechanism between V⁵⁺ and single-electron-trapped oxygen vacancy. *Appl. Catal. B Environ.* **2015**, *176–177*, 160–172. [[CrossRef](#)]
36. Martínez Vargas, D.X.; Rivera De la Rosa, J.; Lucio-Ortiz, C.J.; Hernández-Ramirez, A.; Flores-Escamilla, G.A.; Garcia, C.D. Photocatalytic degradation of trichloroethylene in a continuous annular reactor using Cu-doped TiO₂ catalysts by sol–gel synthesis. *Appl. Catal. B Environ.* **2015**, *179*, 249–261. [[CrossRef](#)]
37. Asahi, R.; Morikawa, T.; Irie, H.; Ohwaki, T. Nitrogen-Doped Titanium Dioxide as Visible-Light-Sensitive Photocatalyst: Designs, Developments, and Prospects. *Chem. Rev.* **2014**, *114*, 9824–9852. [[CrossRef](#)] [[PubMed](#)]
38. Zou, M.; Xiong, F.; Ganeshraja, A.S.; Feng, X.; Wang, C.; Thomas, T.; Yang, M. Visible light photocatalysts (Fe, N):TiO₂ from ammonothermally processed, solvothermal self-assembly derived Fe-TiO₂ mesoporous microspheres. *Mater. Chem. Phys.* **2017**, *195*, 259–267. [[CrossRef](#)]
39. Gole, J.L.; Prokes, S.M.; Glembocki, O.J.; Wang, J.; Qiu, X.; Burda, C. Study of concentration-dependent cobalt ion doping of TiO₂ and TiO_{2-x}N_x at the nanoscale. *Nanoscale* **2010**, *2*, 1134–1140. [[CrossRef](#)] [[PubMed](#)]
40. Yu, J.; Xiang, Q.; Zhou, M. Preparation, characterization and visible-light-driven photocatalytic activity of Fe-doped titania nanorods and first-principles study for electronic structures. *Appl. Catal. B Environ.* **2009**, *90*, 595–602. [[CrossRef](#)]
41. Tong, T.; Zhang, J.; Tian, B.; Chen, F.; He, D. Preparation of Fe³⁺-doped TiO₂ catalysts by controlled hydrolysis of titanium alkoxide and study on their photocatalytic activity for methyl orange degradation. *J. Hazard. Mater.* **2008**, *155*, 572–579. [[CrossRef](#)] [[PubMed](#)]
42. Zhou, M.; Yu, J.; Cheng, B.; Yu, H. Preparation and photocatalytic activity of Fe-doped mesoporous titanium dioxide nanocrystalline photocatalysts. *Mater. Chem. Phys.* **2005**, *93*, 159–163. [[CrossRef](#)]
43. Ohno, T.; Sarukawa, K.; Tokieda, K.; Matsumura, M. Morphology of a TiO₂ Photocatalyst (Degussa, P25) Consisting of Anatase and Rutile Crystalline Phases. *J. Catal.* **2001**, *203*, 82–86. [[CrossRef](#)]

44. Pignatello, J.J.; Oliveros, E.; MacKay, A. Advanced Oxidation Processes for Organic Contaminant Destruction Based on the Fenton Reaction and Related Chemistry. *Crit. Rev. Environ. Sci. Technol.* **2006**, *36*, 1–84. [[CrossRef](#)]
45. Schwenzer, B.; Wang, L.; Swensen, J.S.; Padmaperuma, A.B.; Silverman, G.; Korotkov, R.; Gaspar, D.J. Tuning the Optical Properties of Mesoporous TiO₂ Films by Nanoscale Engineering. *Langmuir* **2012**, *28*, 10072–10081. [[CrossRef](#)] [[PubMed](#)]
46. Grosvenor, A.P.; Kobe, B.A.; Biesinger, M.C.; McIntyre, N.S. Investigation of multiplet splitting of Fe 2p XPS spectra and bonding in iron compounds. *Surf. Interface Anal.* **2004**, *36*, 1564–1574. [[CrossRef](#)]
47. Fan, J.-X.; Wang, Y.-J.; Fan, T.-T.; Dang, F.; Zhou, D.-M. Effect of aqueous Fe(II) on Sb(V) sorption on soil and goethite. *Chemosphere* **2016**, *147*, 44–51. [[CrossRef](#)] [[PubMed](#)]
48. Yamashita, T.; Hayes, P. Analysis of XPS spectra of Fe²⁺ and Fe³⁺ ions in oxide materials. *Appl. Surf. Sci.* **2008**, *254*, 2441–2449. [[CrossRef](#)]
49. Mielczarski, J.A.; Atenas, G.M.; Mielczarski, E. Role of iron surface oxidation layers in decomposition of azo-dye water pollutants in weak acidic solutions. *Appl. Catal. B Environ.* **2005**, *56*, 289–303. [[CrossRef](#)]
50. Orozco, S.L.; Bandala, E.R.; Arancibia-Bulnes, C.A.; Serrano, B.; Suárez-Parra, R.; Hernández-Pérez, I. Effect of iron salt on the color removal of water containing the azo-dye reactive blue 69 using photo-assisted Fe(II)/H₂O₂ and Fe(III)/H₂O₂ systems. *J. Photochem. Photobiol. A Chem.* **2008**, *198*, 144–149. [[CrossRef](#)]
51. Nie, Y.; Hu, C.; Qu, J.; Zhou, L.; Hu, X. Photoassisted Degradation of Azodyes over FeO_xH_{2x-3}/Fe⁰ in the Presence of H₂O₂ at Neutral pH Values. *Environ. Sci. Technol.* **2007**, *41*, 4715–4719. [[CrossRef](#)] [[PubMed](#)]
52. Gutowska, A.; Kałużna-Czaplińska, J.; Józwiak, W.K. Degradation mechanism of Reactive Orange 113 dye by H₂O₂/Fe²⁺ and ozone in aqueous solution. *Dyes Pigment.* **2006**, *74*, 41–46. [[CrossRef](#)]
53. Lin, W.; Frei, H. Photochemical and FT-IR Probing of the Active Site of Hydrogen Peroxide in Ti Silicalite Sieve. *J. Am. Chem. Soc.* **2002**, *124*, 9292–9298. [[CrossRef](#)] [[PubMed](#)]
54. Fenton, H.J.H. LXXIII.-Oxidation of tartaric acid in presence of iron. *J. Chem. Soc. Trans.* **1894**, *65*, 899–910. [[CrossRef](#)]
55. Bandara, J.; Morrison, C.; Kiwi, J.; Pulgarin, C.; Peringer, P. Degradation/decoloration of concentrated solutions of Orange II. Kinetics and quantum yield for sunlight induced reactions via Fenton type reagents. *J. Photochem. Photobiol. A Chem.* **1996**, *99*, 57–66. [[CrossRef](#)]
56. Liang, X.; Zhong, Y.; Zhu, S.; Zhu, J.; Yuan, P.; He, H.; Zhang, J. The decolorization of Acid Orange II in non-homogeneous Fenton reaction catalyzed by natural vanadium–titanium magnetite. *J. Hazard. Mater.* **2010**, *181*, 112–120. [[CrossRef](#)] [[PubMed](#)]
57. Neyens, E.; Baeyens, J. A review of classic Fenton's peroxidation as an advanced oxidation technique. *J. Hazard. Mater.* **2003**, *98*, 33–50. [[CrossRef](#)]
58. Lopez, T.; Moreno, J.A.; Gomez, R.; Bokhimi, X.; Wang, J.A.; Yee-Madeira, H.; Pecchi, G.; Reyes, P. Characterization of iron-doped titania sol-gel materials. *J. Mater. Chem.* **2002**, *12*, 714–718. [[CrossRef](#)]
59. Fallet, M.; Gschwind, R.; Bauer, P. Oxidation States of Iron in Doped TiO₂-SiO₂ Sol-Gel Powders: A ⁵⁷Fe Mössbauer Study. *J. Sol-Gel Sci. Technol.* **2003**, *27*, 167–173. [[CrossRef](#)]
60. Shafia, E.; Esposito, S.; Manzoli, M.; Chiesa, M.; Tiberto, P.; Barrera, G.; Menard, G.; Allia, P.; Freyria, F.S.; Garrone, E.; Bonelli, B. Al/Fe isomorphous substitution versus Fe₂O₃ clusters formation in Fe-doped aluminosilicate nanotubes (imogolite). *J. Nanoparticle Res.* **2015**, *17*, 336. [[CrossRef](#)]
61. Kho, Y.K.; Iwase, A.; Teoh, W.Y.; Mädler, L.; Kudo, A.; Amal, R. Photocatalytic H₂ Evolution over TiO₂ Nanoparticles. The Synergistic Effect of Anatase and Rutile. *J. Phys. Chem. C* **2010**, *114*, 2821–2829. [[CrossRef](#)]
62. Segneanu, A.E.; Orbeci, C.; Lazau, C.; Sfirloaga, P.; Vlazan, P.; Bandas, C.; Grozescu, I. Waste Water Treatment Methods. In *Water Treatment*; Elshorbagy, W., Chowdhury, R.K., Eds.; InTech: Rijeka, Croatia, 2013.
63. Feng, J.; Wong, R.S.K.; Hu, X.; Yue, P.L. Discoloration and mineralization of Orange II by using Fe³⁺-doped TiO₂ and bentonite clay-based Fe nanocatalysts. *Catal. Today* **2004**, *98*, 441–446. [[CrossRef](#)]
64. Mangayayam, M.; Kiwi, J.; Giannakis, S.; Pulgarin, C.; Zivkovic, I.; Magrez, A.; Rtimi, S. FeO_x magnetization enhancing *E. coli* inactivation by orders of magnitude on Ag-TiO₂ nanotubes under sunlight. *Appl. Catal. B Environ.* **2017**, *202*, 438–445. [[CrossRef](#)]

